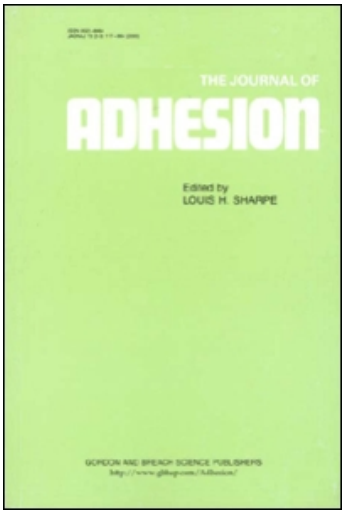

The Journal of Adhesion
Publication details, including instructions for authors and subscription information:
http://www.informaworld.com/smpp/title~content=t713453635

First Principles Study of the Aluminum-Cubic Boron Nitride Interface

Newton Ooi[a]; Louis G. Hector Jr.[b]; James B. Adams[c]; Daniel Stanzione Jr.[d]
[a] Center for Solid State Science, Arizona State University, Tempe, Arizona, USA [b] Materials and Processes Laboratory, General Motors Research and Development Center, Warren, Michigan, USA [c] Department of Chemical and Materials Engineering, Arizona State University, Tempe, Arizona, USA [d] Fulton High Performance Computing, Ira A. Fulton School of Engineering and Applied Sciences, Arizona State University, Tempe, Arizona, USA

To cite this Article Ooi, Newton , Hector Jr., Louis G. , Adams, James B. and Stanzione Jr., Daniel(2006) 'First Principles Study of the Aluminum-Cubic Boron Nitride Interface', The Journal of Adhesion, 82: 8, 779 — 803
To link to this Article: DOI: 10.1080/00218460600822716
URL: http://dx.doi.org/10.1080/00218460600822716

The Journal of Adhesion, 82:779–803, 2006

ISSN: 0021-8464 print/1545-5823 online
DOI: 10.1080/00218460600822716

Taylor & Francis
Taylor & Francis Group

First Principles Study of the Aluminum–Cubic Boron Nitride Interface

Newton Ooi
Center for Solid State Science, Arizona State University, Tempe, Arizona, USA

Louis G. Hector Jr.
Materials and Processes Laboratory, General Motors Research and Development Center, Warren, Michigan, USA

James B. Adams
Department of Chemical and Materials Engineering, Arizona State University, Tempe, Arizona, USA

Daniel Stanzione Jr.
Fulton High Performance Computing, Ira A. Fulton School of Engineering and Applied Sciences, Arizona State University, Tempe, Arizona, USA

A plane wave density functional methodology, with the local density approximation for the elemental constituents, was used to investigate the structure, bonding, and adhesion of atomic-scale interfaces between aluminum and cubic-boron nitride (c-BN). Two fully periodic interfaces, Al(110)–c-BN(110) and Al(001)–c-BN(110), were constructed for this purpose. Interfacial bonding, examined with contours of the charge density difference and electron localization function, was found to be stronger between Al–N pairs than Al–B pairs. The computed work of separation (W_s) values were 2.25 J/m^2 for Al(110)–c-BN(110) and 2.65 J/m^2 for Al(001)–c-BN(110). The higher adhesion in the latter interface is attributed to a higher planar density of interfacial Al atoms. The computed W_s values were compared with values from first principles calculations on other aluminum–ceramic interfaces. The possibility of adhesive transfer during tensile debonding was qualitatively investigated.

Keywords: Aluminum; Cubic boron nitride; Density functional; Interface structure; Simulation

Received 16 February 2006; in final form 4 May 2006.

Address correspondence to Newton Ooi, Center for Solid State Science, Box 871704, Arizona State University, Tempe, AZ 85287-1704, USA. E-mail: newtonooi@hotmail.com

1. INTRODUCTION

Crystalline boron nitride is a synthetic material that exists in both cubic (c-BN) and hexagonal phases (h-BN). The cubic form (also referred to as borazon), with the $F\bar{4}3\,m$ (zincblende) space group and room temperature lattice constant $a_0 = 3.615\,\text{Å}$ [1], is isostructural with diamond. The extreme hardness of c-BN is derived from its periodic array of tetrahedral-oriented, covalent (sp^3-hybridized) bonds between B and N [2]. Unlike diamond, however, c-BN is particularly useful as a cutting material for ferrous metals because it does not react with these materials. Over the past decade, there has been substantial interest in the preparation of BN thin films for tribological applications. However, a careful review of the literature revealed no commercially viable (crystalline) c-BN thin film used as a tribological coating in metal fabrication processes (*e.g.*, machining). Many of the extant films are largely mixtures of the cubic and hexagonal phases (vapor-phase deposition techniques typically produce nanocrystalline films), and we surmise that low-defect density, crystalline c-BN films are unavailable at the present time largely for this reason [3–8]. Hence, there is essentially no information that would suggest how c-BN might perform as a coating material in various aluminum manufacturing processes, for example, wherein the native oxide [9] is damaged, resulting in exposure of nascent metal, which is highly chemically reactive. This is intriguing because theoretical studies suggest that nascent aluminum does not adhere to hydrogen-terminated (unreconstructed) diamond and perhaps hydrogenated diamond-like carbon [10], which consists of C−C bonds in sp^2 and sp^3 hybridization. Theoretical investigation of c-BN adhesion is of interest because it represents a limiting case for the mixed cubic and hexagonal phases.

In the absence of commercially viable crystalline c-BN films, first principles modeling studies can provide a unique understanding of bonding and adhesion of c-BN to metallic surfaces. Many of the existing studies have employed density functional theory (DFT) with appropriate exchange and correlation functionals and pseudopotentials for the elemental constituents. Beyond those investigations that have focused solely on electronic structure (*i.e.*, ground state) and bonding in c-BN [9–12], the most frequently studied interface is c-BN–diamond. This is likely due to the similarity in lattice constants and crystal structures of these materials, which makes construction of a c-BN–diamond atomistic-scale interface fairly straightforward. For example, diamond(110)–c-BN(110) was investigated by Pickett [13] to determine the band structure and other electronic properties of the interface. Periodic sandwich models of the type nC–nBN were

studied, where n = 1, 3, and 5 atomic planes. Lattice mismatch was minimized by setting $a_0 = 3.589$ Å for both materials. Using the linear muffin tin orbital approach (LMTO) with the local density approximation (LDA), Lambrecht and Segall [14,15] investigated the same interface using a sandwich model of the form 2nC–nBN, where again n is the number of atomic planes and varies as 1, 3, 5 . . .. The density of states, interface energy, charge distribution, and band structure were calculated for each interface. Neither investigation explicitly calculated the surface energy of c-BN(110), although Lambrecht and Segall [14,15] provided an estimate of 0.9 eV/atom using a simple bond-breaking model. Yamamoto *et al.* [16] modeled an interface consisting of five layers of both C(110) and c-BN(110). The charge density and total potential were computed as a function of position from the interface. The charge density (potential) was lower (higher) in the c-BN slab than in the diamond slab, indicating charge transfer from the c-BN to the diamond. He *et al.* [17] studied the diamond(001)–c-BN(001) polar interface using the generalized gradient approximation (GGA). Both B- and N-terminated interfaces were examined to determine the preferred termination. Energy comparisons between this interface and the diamond(110)–c-BN(110) interface investigated in Refs. 13–16 show that the (001) interface is less stable with a positive formation energy.

Other theoretical studies have focused on bonding between c-BN and group IV materials. For example, Benzair and Aourag [18] modeled interfaces of c-BN(001) and the (001) surfaces of SiC, GeC, and SnC. Wang *et al.* [19] used the LMTO method with the LDA to examine the c-BN(001)–SiC(001) interface and found evidence of preferred Si–N and B–C bonds. Zhang *et al.* [20] studied adsorption of B and N atoms on Al(001) using a local basis set within the DFT framework. The Al(001) was represented using cluster models of different geometries. A boron atom was placed at various points above the cluster surface, and the energy was calculated at each point. They found that both N and B form covalent bonds with the Al surface, but N bonds more strongly to Al than B. In both cases, the ad-atom preferred to sit in the interstitial region between adjacent Al atoms, instead of directly above an Al atom.

In contrast to the growing literature on interfaces between c-BN and semiconducting materials, there is minimal literature on metal–c-BN interfaces. One experimental study examined the coefficient of friction between c-BN films and aluminum balls in various atmospheres, but no information on adhesion or interfacial energies was offered [21]. Adhesion of liquid aluminum (as well as other liquid metals) to c-BN was measured in Refs. [22,23]. A 78° wetting angle,

$0.943\,J/m^2$ work of adhesion, and a $4.538\,J/m^2$ surface energy on a polycrystalline c-BN surface were reported. The orientation of the c-BN surface was not specified, and hence, little can be deduced about the influence of c-BN surface termination on adhesion.

We employed DFT using the LDA to investigate the structure and adhesion of model Al(110)–c-BN(110) and Al(001)–c-BN(110). Aluminum was chosen as the metallic surface material because of its extreme chemical affinity and its technological importance. To benchmark our procedure, we first conducted bulk calculations on each material and then computed surface energies of the isolated Al slabs, referring to recently published results for comparable information on c-BN(110) slabs. Fully periodic cells were then constructed with inversion symmetry so as to guarantee identical chemical and geometrical environments in the two interfaces contained therein. Interfacial registry in the cells was imperfect because of the large lattice mismatch between Al and c-BN. The work of separation, W_s, was then calculated for both interfaces, and bonding was explored by computing and displaying the charge density difference and electron localization functions in specific cell planes.

The remainder of this article is organized as follows. We discuss our computational approach in Section 2. Results from bulk and surface energy calculations on the isolated Al and c-BN(110) slabs are discussed in Section 3. Construction of the interface is outlined in Section 4, and our adhesion calculations are presented in Section 5. In Section 6, the minimized interface structures are described. Interfacial bonding is explored in Section 7, and we review the major results of the work in Section 8.

2. COMPUTATIONAL PROCEDURE

Total energies and minimized cell geometries were computed with the Vienna Ab Initio Simulation Package (VASP V4.6) [24,25]. In VASP, the Kohn–Sham orbitals are expanded in a plane-wave basis and used in conjunction with projected augmented wave (PAW) [26,27] (all-electron) potentials for the elemental constituents. The LDA, parameterized by Ceperley and Alder [28], was used for the exchange and correlation functional because this has been the choice of many previous electronic structure investigations involving BN (the GGA functional could have just as easily been used in the present work). Reported calculations on Al–graphite interfaces used the LDA functional [29], and for those few studies where the W_s values from LDA and GGA were compared, differences of the order of 12% or less were noted [30]. Initial charge densities were taken as a superposition of atomic charge

densities. The cutoff energies (valence configurations) for the Al, B, and N LDA PAW potentials were 240.96 eV ($2s^2p^1$), 318.76 eV ($3s^2p^1$), and 400 eV ($2s^2p^3$), respectively. A 410-eV cutoff energy was used for all interface calculations. Energies and charge densities were calculated self-consistently using a Pulay-like charge mixing scheme [31] and the blocked Davidson [32,33] minimization algorithm. Energy convergence was achieved at 10^{-6} eV/cell. Ionic positions were relaxed to the ground state by minimizing the Hellman–Feynman forces [34,35] using a conjugate gradient algorithm such that all the atomic force components were less than 0.05 eV/Å. Because our interfaces were quite large (*i.e.*, in excess of 540 ions), computational cost was minimized by sampling the irreducible Brillouin Zone (BZ) at the Γ-point, which was sufficient to converge the energy and ionic forces to the stated tolerances. The single k-point precluded the use of tetrahedron methods [36] for BZ integration. Hence, the step function at the Fermi level was smoothened using a 0.01-eV Gaussian broadening parameter. The cell parameters and ionic degrees of freedom were simultaneously optimized with the VASP code.

3. BULK AND SURFACE RESULTS

There is minimal experimental data for c-BN surface properties, with a few publications suggesting that the {110} planes are the preferred cleavage planes of c-BN [37]. This makes sense because the c-BN{110} are the only surfaces that are stoichiometric B:N. The other surfaces are either B or N terminated, which introduces surface polarity. The bulk and (110) surface properties of c-BN were previously examined [38], and those results showed that a five-layer slab of c-BN(110) was thick enough to converge the surface energy, σ, to less than 0.1 J/m^2 (see Ref. [29] for a discussion of the surface energy). Therefore, a five-layer slab is predicted to have a bulk-like interior.

To determine the efficacy of the LDA PAW for modeling Al, calculations were performed to obtain its single-crystal bulk modulus, B_0; cohesive energy, E_C; and the lattice constant, a_0. This was followed by surface calculations to determine the slab thickness for the three low-index Al surfaces: {111}, {001}, and {110}. Using a 1-atom primitive cell for the bulk, **k**-point convergence to 1 meV/atom was achieved with a $10\times10\times10$ mesh and 110 irreducible points. Plane wave convergence to 1 meV/atom was achieved at 260 eV. The cell energy variation with a_0 was obtained by varying a_0 incrementally from 3.9 to 4.1 Å, calculating the energy at each a_0 increment, and fitting the resulting curve to the Birch–Murnaghan [39,40] equation of state to determine E_C, B_0, and a_0. Comparisons between calculated and literature values

TABLE 1 Comparison between Calculated and Literature Values of Aluminum Properties

Reference at (temperature)	Data type	B_0 (GPa)	a_0 (Å)	E_C (eV/ion)
[41] (300 K)	Experimental	76	4.0495	—
[42] (300 K)	Experimental	72.2	4.0495	3.39
[43] (0 K)	Calculated	80.9	4.032	3.36
[44] (0 K)	Calculated	79.4	4.032	—
Present calculations	Calculated	83.27	3.985	4.053

are listed in Table 1. The LDA overbinds, producing E_C and B_0 values slightly higher than the experiment, and a_0 values slightly lower than the experiment.

The 1×1 models for each low-index Al surface are given in Table 2 in terms of a_0 and are shown in Figure 1. Vectors U and V run parallel to the surface plane and define the 1×1 primitive cell of the slab. Vacuum convergence to 0.01 eV/atom was reached at 10 Å. K-point convergence was reached with a 15×15×2 k-mesh or smaller for all three surfaces, corresponding to 36, 64, and 54 points in the irreducible BZ for the (001), (110), and (111) slabs, respectively. Slab thickness convergence tests were conducted for all three surfaces. For each slab, the energy was obtained on the as-built slab. The atom positions were then minimized, keeping the cell parameters fixed. A final energy was obtained on the minimized slab. The σ was calculated on both as-built and minimized slabs at each slab thickness as the

TABLE 2 Parameters for 1×1 Slabs of the Three Low-Index Surfaces of Aluminum

	Surface		
Parameter	{001}	{111}	{110}
Stacking sequence	AB	ABC	AB
Vector U	$a_0/\sqrt{2}$	$a_0/\sqrt{2}$	a_0
Vector V	$a_0/\sqrt{2}$	$a_0/\sqrt{2}$	$a_0/\sqrt{2}$
Area of one surface	U∗V	$0.5{*}U{*}V{*}\sqrt{3}$	U∗V
Angle between U and V	90°	60 or 120°	90°
Interplanar spacing	$a_0/2$	$a_0/\sqrt{3}$	$a_0\sqrt{2/4}$
Cell type	Tetragonal	Hexagonal	Orthorhombic
Atoms per layer	1	1	1
Point symmetry	C_4v	C_3v	C_2v
Point group	D_4h	D_3d	D_2h

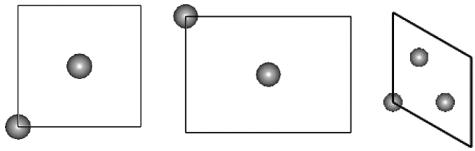

FIGURE 1 Normal views of the 1×1 Al surfaces. From left to right, they are the (001), (110), and (111).

difference between the energy of that slab and the energy of the slab without vacuum divided by the area of both surfaces.

The slab thickness was converged to less than 0.03 J/m^2 at seven to eight layers for the (001), eight to nine layers for the (110), and seven layers for the (111); see Table 3. Calculated values are compared with literature values in Table 4. There are no 0 K experimental σ-values for any surface, but there are many reports of σ for polycrystalline Al and for specific surface facets at finite temperatures. These are in

TABLE 3 Calculated σ (J/m^2) of Low-Index 1×1 Al Surfaces

Slab thickness (layers)	(001)		(110)		(111)	
	As-built	Relaxed	As-built	Relaxed	As-built	Relaxed
1	1.224	1.224	1.360	1.360	1.029	1.029
2	1.147	1.146	1.239	1.109	0.923	0.912
3	1.080	1.080	1.129	1.125	0.879	0.879
4	1.058	1.055	1.071	1.052	0.928	0.927
5	1.050	1.051	1.116	1.063	0.881	0.879
6	1.013	1.007	1.179	1.120	0.855	0.853
7	0.998	0.985	1.157	1.110	0.847	0.845
8	0.996	0.987	1.088	1.061	0.819	0.817
9	1.004	0.989	1.079	1.052	0.785	0.784

TABLE 4 Literature Values for the Al Surface Energies (J/m^2)

Ref.	Data type	(001)	(110)	(111)	Polycrystalline
[45]	DFT calc.	0.89	—	0.81	—
[46]	DFT calc.	0.977	1.103	0.921	—
[47]	DFT calc.	—	—	1.27	—
[48]	DFT calc.	1.347	1.271	1.199	—
[49]	DFT calc.	—	1.230	—	—
[50]	Experimental	0.977–1.347	1.103–1.271	0.921–1.199	1.1–1.2

the range of 0.8–1.3 J/m^2, and publications that give specific values for different facets typically report the (111) surface as having the lowest σ. The (111) surfaces of FCC metals (like Al) have been demonstrated experimentally [51] and theoretically [52] to have the lowest σ-values, suggesting that they are the energetically preferred terminations. Our calculated values are similar to both experimental and other calculated values, with the (111) σ value being the lowest value, so we believe them to be reliable.

4. INTERFACE CONSTRUCTION

Interfaces between c-BN(110) and Al(111), Al(001), and Al(110) were constructed following slab thickness determination. The c-BN(110), Al(001), and Al(110) slabs are rectangular; therefore, the Al(001)–c-BN and Al(110)–c-BN are the smallest interfaces (*i.e.*, fewest atoms) with the smallest lattice mismatch; calculations were performed on these structures. Both Al–c-BN(110) interfaces were constructed as follows.

1. Create extended Al and c-BN surfaces using the experimental lattice constants.
2. Match up the Al surface with c-BN(110) such that a multiple of the (1×1) Al surface cell approximately matches up with a multiple of the (1×1) c-BN surface cell. The resulting interfaces are 5×5 Al(110)–4×8 c-BN(110) and 5×7 Al(001)–4×8 c-BN(110).
3. Reduce the lattice mismatch to under 0.01 Å by varying the lattice constants for both Al and c-BN. From the LDA PAW calculations, $B_0 \approx 335$ GPa for c-BN while $B_0 \approx 82$ GPa for Al. The ratio of the two is ~0.24, and hence c-BN is ~four times harder than Al. Therefore, to minimize lattice mismatch, the Al lattice constant was varied by ± 0.1 Å from its calculated value, and the c-BN lattice constant was varied by ± 0.025 Å from its calculated value. The final lattice mismatch was under 0.0001 Å (0.0001%).
4. The thicknesses of the c-BN and Al slabs were taken from their surface calculations.

The interfaces are periodic with no vacuum except for the small separation between the two slabs. Parameters associated with the as-constructed interfaces are listed in Table 5; the number of decimal places listed is equal to the number used in constructing the interface. Both structures have two interface planes identical in chemistry and geometry, so the interface has two mirror planes parallel to the interface plane. Assuming that the Al slab, (001) or (110), has ABAB stacking and the c-BN slab has CDCD stacking, the stacking sequence

TABLE 5 Parameters for the Al–c-BN Interfaces

	5×7 Al (001)–4×8 BN (110)		5×5 Al (110)–4×8 BN (110)	
Parameter	Al	BN	Al	BN
Experimental a_0 at 300 K (Å)	4.0495	3.615	4.0495	3.615
Calculated a_0 (Å)	3.987	3.584	3.987	3.584
a_0 used for interface construction (Å)	4.0275	3.5600	4.034212	3.565773
Slab thickness (layers)	7	5	9	5
Atoms per 1×1 layer	1	2	1	2
No. of 1×1 units in one layer	5∗7 = 35	4∗8 = 32	5∗5 = 25	4∗8 = 32
Atoms per entire layer	35∗1 = 35	32∗2 = 64	25∗1 = 25	32∗2 = 64
Atoms per slab	35∗7 = 245	64∗5 = 320	25∗9 = 225	64∗5 = 320
Point symmetry of slab	C_1	C_1h	C_1	C_1h
Point group of slab	C_1h	C_2v	C_1h	C_2v
Atoms in entire interface model	245 + 320 = 565		225 + 320 = 545	
Interface width: U	14.2400 Å		14.2400 Å	
Interface length: V	20.1384 Å		20.1384 Å	
Area of one interface = U∗V	286.7708 $Å^2$		286.7708 $Å^2$	
Point symmetry of interface	C_1		C_1	
Point group of interface	C_1h		C_1h	
Stacking sequence of interface	ABA**B**ABA–CD**C**DC		ABAB**A**BABA–CD**C**DC	

at the Al(110)–c-BN(110) interface is then ABABABABA–CDCDC. In Table 5, the atomic layers that are mirror planes parallel to the interface plane are listed in **bold-faced** type and underlined within the listed stacking sequences. The interface geometries are shown in Figure 2. We did not investigate interfaces formed using the reconstructed c-BN(110) surface because the dimensions of the unreconstructed (110) slab used to create the interface do not geometrically restrict any surface reconstruction.

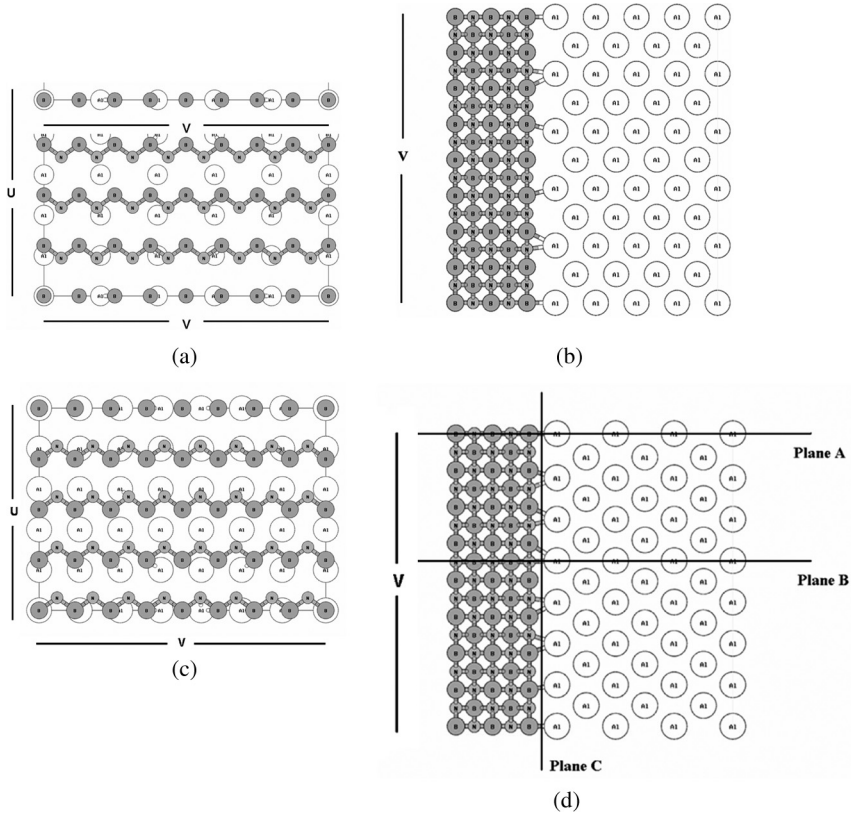

FIGURE 2 Al–c-BN interfaces. The biggest atoms are Al, followed in size by B atoms and N atoms. Where appropriate, the dimensions U and V are labeled besides the Al(110)–c-BN(110): side view structure. a) Al(110)–c-BN(110): view of atoms at the interface plane only; b) Al(110)–c-BN(110): side view; c) Al(001)–c-BN(110): view of atoms at the interface plane only; and d) Al(001)–c-BN(110): side view; labeled planes are referred to in Figures 6 and 7.

Other Al–c-BN(110) interface geometries could be generated by sliding or rotating one surface with respect to the other surface parallel to the interface plane. We did not do this for three reasons. First, this would have resulted in much larger interface models, making the calculations computationally prohibitive. Second, our interface models have minimal mismatch of lattice distances and zero mismatch of lattice angles: this minimizes the sensitivity of the total energy of each interface to the amount of lattice mismatch. Because our interfaces were constructed with very minimal lattice mismatch, other structures that might result from translation or rotation of the slabs along the interface are unlikely to result in an even smaller mismatch. Finally, both of our constructed interfaces are large enough that they include various geometries of different Al–B and Al–N relative positions. Along with lattice mismatch, the total energy of an interface depends upon the relative positioning of different atoms across the interface. Each of our models already includes different relative positioning of metal–ceramic atoms at the interface. Alternative interface models would be larger and might include additional positioning of metal–ceramic atoms, which would not lead to a lower total energy.

5. ADHESION CALCULATIONS

The thermodynamic work of adhesion, ω_a, is the free energy needed to reversibly separate an interface into two free surfaces. This is described by the Dupré Equation (1), where σ_x is the surface energy of material X in equilibrium with its vapor phase and γ is the interface energy. Wetting experiments give values of ω_a as an energy per area. A related term is the (nonequilibrium) work of separation, W_s. This is the energy needed to reversibly separate an interface into two free surfaces, ignoring plastic and diffusion degrees of freedom. Plastic degrees of freedom include grain boundary sliding, twinning, dislocation motion, or bond breaking in the bulk of either material and can be large for systems that undergo significant plastic deformation. The W_s can be calculated by replacing the equilibrium surface energies in the Dupré equation [53] by their instantaneous values prior to equilibrating with the atmosphere. The W_s is defined in Equation 2 where the interface area is A, γ is the interface energy, and E_T is the total energy of the system. The instantaneous σ of material X is σ_x, and E_X is the total energy of X.

$$\omega_a = \sigma_1 + \sigma_2 - \gamma \tag{1}$$

$$W_s = \sigma_1 + \sigma_2 - \gamma = \frac{E_1 + E_2 - E_T}{A} \tag{2}$$

The large number of atoms in each interface cell requires computationally expensive geometry minimizations (*i.e.*, relaxation of the electronic and nuclear degrees of freedom). One way to reduce the computational cost is to determine the optimal interfacial separation ($\triangle$) *a priori*, thereby reducing the distance the slabs have to move during a geometry minimization. The energy of the entire interface was calculated at different values of $\triangle$ from 1.5 Å to 4 Å. From the plot of γ *versus* $\triangle$ given in Figure 3, we note that γ is minimized at interfacial separations of 1.83 Å and 1.90 Å for the Al(110)–c-BN(110) and Al(001)–c-BN(110), respectively. The interface energy is obtained from DFT calculations using Equation 3 below where n_{Al}, n_B, and n_N are the number of Al, B, and N atoms in the interface model; E_{Al} is the energy per atom in bulk Al; and $E_{c\text{-}BN}$ is the energy per atom in bulk c-BN. The area of one interface plane is A.

$$\gamma = \frac{E_T - n_{Al}E_{Al} - (n_B + n_N)E_{c-BN}}{A} \tag{3}$$

Two values of the W_s were computed for each interface. The first value resulted from single-point energy calculations on the as-constructed interface cells (following adjustment of the initial interfacial separations) and on the as-built Al and c-BN slabs associated

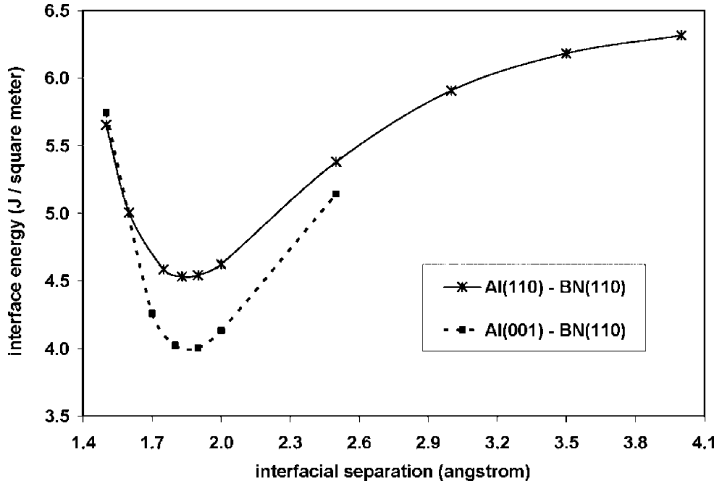

FIGURE 3 Interface energy as a function of separation between rigid Al and c-BN slabs.

TABLE 6 Summary of Al–c-BN Interface Calculations

Interface	Type	Δ (Å)	W_S (J/m^2)
Al (110)–c-BN (110)	As-built	1.83	9.12
	Minimized	1.72	2.25
Al (001)–c-BN (110)	As-built	1.90	2.32
	Minimized	1.99	2.65

with each cell. The second W_s value resulted from simultaneous geometry and cell parameter optimizations on the as-constructed interfaces. Single-point energies were then calculated for the slabs from the fully minimized interfaces. These values are listed in Table 6 and show a large difference in W_s between the as-built and minimized interfaces for Al(110)–c-BN(110). The W_s changes for both interfaces after minimization because of the relaxation of atoms. A large change in W_s upon minimization is expected when the surfaces in the interface undergo large relaxations or reconstructions. This is the case here as both the c-BN(011) and Al surfaces undergo relaxations or reconstructions, which have been detailed experimentally. The interface geometry is studied further in the next section.

Table 7 contains results computed for other adhesion pairs involving Al. Our computed W_s values for Al–c-BN are intermediate to those computed previously for Al–VC (vanadium carbide) and Al–WC (tungsten carbide). A strict quantitative comparison is inappropriate because the latter two values were computed with GGA. Suffice it to say that the predicted adhesion values for Al and c-BN are within

TABLE 7 Work of Separation (W_s) Computed with the Same First Principles Methodology for Other Interfaces with Al

Adhesion pair	Orientation	Exchange-correlation	W_S (J/m^2)	Ref.
Al/diamond 1×1:H	$(111)[11\bar{2}]_{Al}\|\|(0001)[10\bar{1}0]_C$	GGA	0.02	[54]
Al/graphite	$(111)[11\bar{2}]_{Al}\|\|(0001)[10\bar{1}0]_C$	LDA	0.11	[55]
Al/diamond 2×1	$(111)[11\bar{2}]_{Al}\|\|(0001)[10\bar{1}0]_C$	GGA	0.33	[54]
Al/VC	$(100)[001]_{Al}\|\|(100)[001]_{VC}$	GGA	2.14	[56]
Al/WC	$(110)[1\bar{1}0]_{Al}\|\|(11\bar{2}0)[0001]_{WC}$	GGA	3.14	[57]
Al/WC^w	$(111)[\bar{1}10]_{Al}\|\|(0001)[11\bar{2}0]_{WC}$	GGA	4.08	[57]
Al/diamond 1×1	$(111)[11\bar{2}]_{Al}\|\|(111)[10\bar{1}]_C$	GGA	4.08	[54]
Al/WC^c	$(111)[\bar{1}10]_{Al}\|\|(0001)[11\bar{2}0]_{WC}$	GGA	6.01	[57]

Note. LDA values typically exceed GGA values for the same interface pair by 10–12%. Subscripts/superscripts denote surface termination species.

the range of those values predicted for Al and VC and those for Al and WC. This is not surprising because VC and WC are covalently bonded conductors (having metallic and ionic bonding character as well) with bulk moduli of 303 GPa and $\sim$400 GPa [30], respectively. It is interesting to note that the smallest W_s ($0.02\,J/m^2$) was found with the hydrogen-terminated diamond 1×1, whereas the largest W_s ($6.01\,J/m^2$) was found with the highly reactive carbon-terminated WC. Tensile debonding simulations in Ref. [58] predicted no adhesive transfer of Al to hydrogen-terminated diamond 1×1, while two contiguous layers of Al transferred to diamond 1×1 (unreconstructed), for which $W_s = 4.08\,J/m^2$. Although we have not performed comparable simulations with our Al–c-BN(110) cells, we expect that some adhesive transfer of Al to c-BN(110) will occur, although the imperfect registry associated with our interfaces may not lead to transfer of contiguous Al layers.

6. MINIMIZED INTERFACE GEOMETRY

The positions and forces on the atoms were analyzed from the minimized interface. Figures 4a and b show the interplanar spacings for the minimized and as-built interfaces. The interplanar spacing is defined as the distance between adjacent planes measured along the direction perpendicular to the interface plane. This can also be interpreted as the difference in heights between adjacent planes, where the height of a plane was taken as the average of the heights of each atom on that plane. For the minimized interface, interplanar spacings were plotted once with the height of each c-BN(110) plane measured using both B and N ion core positions. The c-BN(110) spacings in the minimized interface are also plotted where the height of each (110) plane is measured using B atoms only and once using N atoms only. The plot has been formatted such that the c-BN(110) planes are the middle data points. The Al spacings are on the left and right sides of the c-BN slab.

The interplanar spacings are symmetric about the middle of the Al slab or the middle of the c-BN slab, suggesting that both interfaces remain chemically and structurally identical after minimization. In both the Al and c-BN slabs, the (110) spacings are smallest between the surface and subsurface plane and are largest in the middle of the slab. This indicates that there is an inward relaxation of the surface planes in both slabs. The B atoms at the interface sink into the c-BN slab bulk about 0.05–0.1 Å more than their neighboring N atoms. This height difference between adjacent B and N atoms is likely due to greater attraction between Al and N atoms than Al and B atoms. The

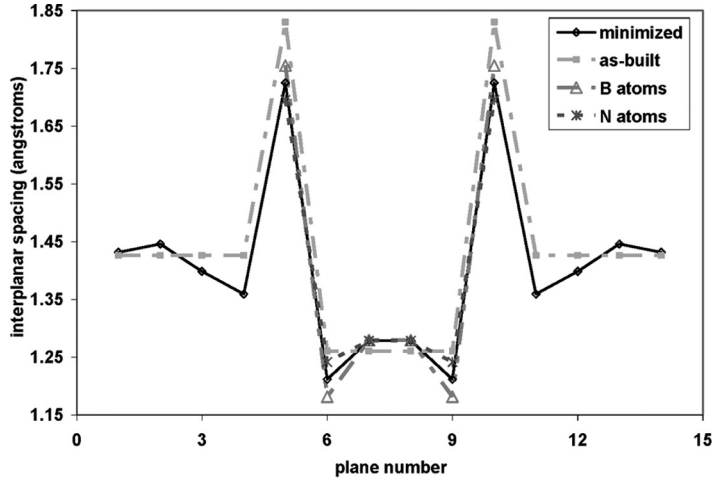

(a)

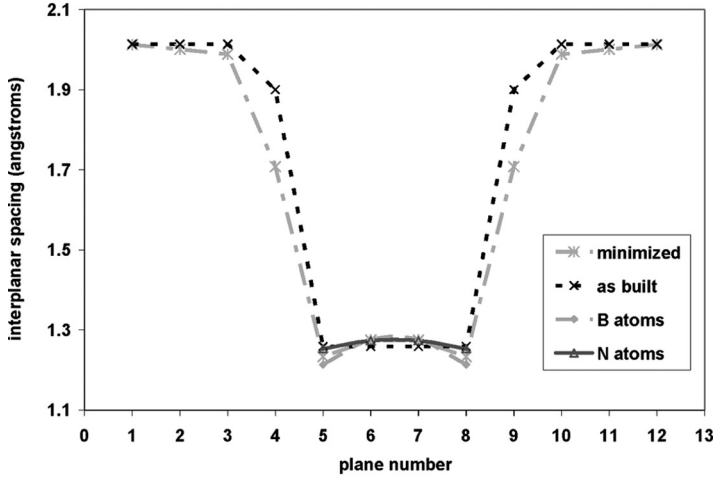

(b)

FIGURE 4 Interplanar spacings in the Al–c-BN interfaces. a) Al(110)–c-BN(110): planes 5–9 are c-BN(110) and planes 1–4 and 10–15 are Al(110); b) Al(001)–c-BN(110): planes 5–9 are c-BN(110) and planes 1–4 and 10–13 are Al(001).

height difference was ~ 0.2 Å for the free c-BN(110) surface and has been reduced at the Al–c-BN interfaces. This reduction is due to interactions with the Al slab. Specifically, Al atoms bond with both B and N

atoms across the interface, thereby making the c-BN(110) plane at the interface more planar than it would be as a free surface.

From Figure 4a, $\triangle = 1.72$ Å ($\triangle = 1.83$ Å) in the minimized Al(110)–c-BN(110) (as-built interface): both are noticeably larger than the (110) spacings in either the Al or c-BN slabs from the minimized interface. This suggests that interfacial bonding is weaker than cohesive bonding in either the c-BN or Al slabs. This is different in the minimized Al(001)–c-BN(110), where $\triangle$ is less than the Al(001) interplanar spacings, but in excess of the c-BN(110) interplanar spacings. Here, the interfacial bonding might be more than the interplanar bonding in the Al slab perpendicular to the interface plane. Therefore, we expect that sufficient tension applied to this interface will lead to separation in the Al slab instead of at the interface.

The planes parallel to the interface plane did not remain flat after geometry minimization. Instead, there was noticeable corrugation in that many of the atoms in the plane were actually above or below the plane. Figure 5 shows the corrugation of each plane as a function of position. The corrugation of a specific atom is defined as the distance between the position of that atom and the position of the plane on which the atom resides, with all positions measured perpendicular to the interface plane. The position of a plane is taken as the average of positions of all the atoms residing in that plane. As is the case for Figure 4, the c-BN(110) planes are in the middle of each figure, with the Al planes on either side. Corrugation was larger for planes closer to the interface than planes in the middle of each slab, which is expected because the slab middle represents a bulk-like interior. Corrugation was greater in the Al slab than in the c-BN slab, which is expected as Al is softer than c-BN. Corrugation was greater in Al(110)–c-BN(110) than in Al(001)–c-BN(110), and this can be related to the smaller equilibrium $\triangle$ value in the former interface than in the latter. Specifically, the closer the c-BN slab is to the Al slab, the less vacuum there is at the interface and the more bulklike the interface region becomes. This in turn reduces the tendency of the Al planes to relax or reconstruct, so the flatter the planes remain, reducing corrugation.

7. INTERFACE BONDING

We examine bonding in Al(001)–c-BN(110) because its W_s exceeded that of Al(011)–c-BN(011) following minimization, and there is a greater number of Al, B, and N ions falling in the same interslab planes than in Al(110)–c-BN(110). We have no reason to believe that the bond character of the two interfaces is significantly different, although

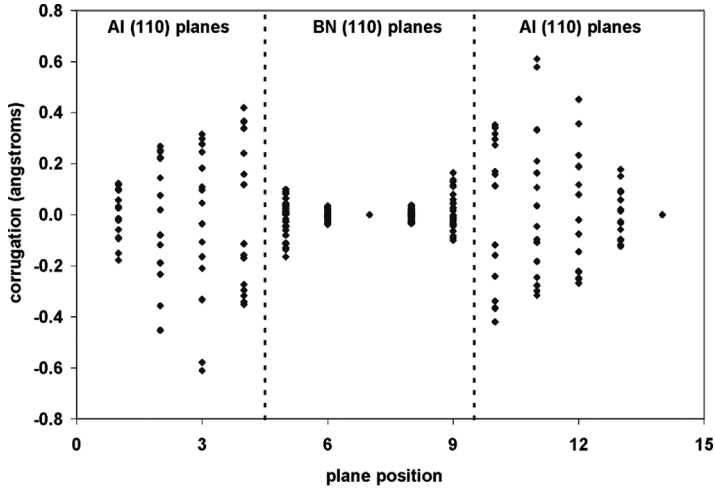

(a)

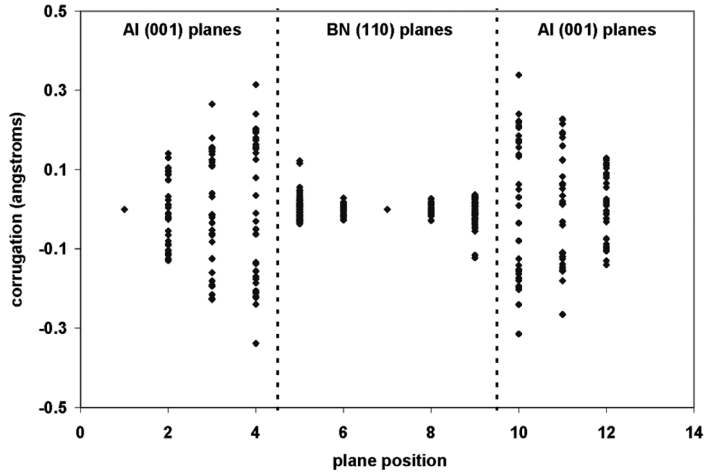

(b)

FIGURE 5 Corrugation of atoms perpendicular to the interface plane in the minimized interfaces: a) Al(110)–c-BN(110); b) Al(001)–c-BN(110).

charge localization will differ because of the Al surface termination and subsequent geometry minimization. We investigated interfacial bonding in the minimized Al(001)–c-BN(110) by computing and displaying contours of the charge density difference (CDD) and the electron localization function (ELF) on planes parallel to and

perpendicular to the interface plane. Both are numerical functions that provide a qualitative, albeit intuitive, feel for bonding; there is no unique partitioning of charge with a plane-wave basis set such as that used here. The CDD results from subtraction of the noninteracting charge density (*i.e.*, due to the isolated ions at their positions in the minimized interface) from the self-consistent charge density. In other words, the difference charge provides a qualitative estimate of charge redistribution when bonding is instantaneously "activated" in the cell. Areas with positive CDD values indicate charge gain and areas with negative CDD indicate charge loss. The ELF was originally developed to elucidate atomic shell structure and bond charge in molecular systems [59] and is especially useful for materials containing first- and second-row elements. ELF values are confined to the $0 < \mathrm{ELF} < 1$ interval; $\mathrm{ELF} = 0.5$ corresponds to electron-gas-like pair probability typical of sp metals; $\mathrm{ELF} = 1.0$ denotes covalent bonding or charge localization. ELF values lack units, whereas the CDD contours have units of electrons per $\mathrm{\AA}^3$.

Figures 6 and 7 show CDD and ELF contours, respectively. In each figure, Al, B, and N ion core positions are denoted by black, white, and gray circles, respectively. Specific values of the CDD and the ELF are listed in the keys associated with each figure. Figures 6a, 6b, 7a, and 7b show contours in planes perpendicular to the interface plane (in all cases this is the region between adjacent Al and c-BN slabs) corresponding to the planes labeled "A" and "B" in Figure 2d. These plots depict how bonding changes when moving from the Al slab, through the interface, and into the c-BN slab. Figures 6a and 7a shows contours in the plane in which Al and B ions are nearest to each other at the interface; this corresponds to a view of plane A in Figure 2d at normal incidence. Figures 6b and 7b show contours in the plane in which the Al and N ions are nearest to each other at the interface; this results from a view of plane B in Figure 2d at normal incidence. Figures 6c and 7c show contours in a plane at the interface and parallel to the interface plane such that no atoms are present (although we project atom positions into the plane in both figures for reference). The views in Figures 6c and 7c are those at normal incidence to plane C in Figure 2d and represent a view looking at the interface plane from inside one of the slabs in the minimized cell. Figures 6a, 6b, 7a, and 7b suggest metallic bonding in Al and localized covalent–ionic bonding in c-BN due to the gray three-leaf, shamrock-like contour lobes about the ions. ELF values are ~ 0.5 (or less) in bulk Al, whereas the near-zero CDD contours suggest minimal charge transfer between different regions of the inner portion of the Al slabs. In the c-BN slab, the CDD contours show charge accumulation in the regions between adjacent B

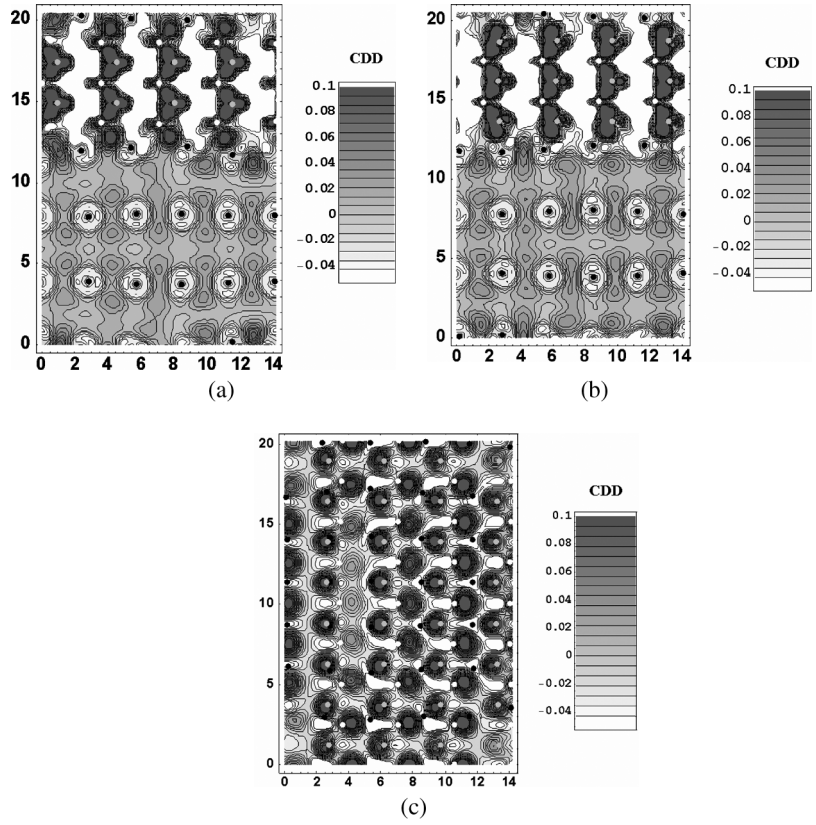

FIGURE 6 CDD plots in the Al(001)–c-BN(110). Dimensions along the sides of the plane denote distance (Å). Al atoms are black; B atoms are white; N atoms are gray. Planes A, B, and C are diagrammed in Figure 2d. a) plane A: Al surface atoms are closest to B surface atoms; b) plane B: Al surface atoms are closet to N surface atoms; c) plane C: plane residing in interface vacuum directly between Al and c-BN slabs.

and N atoms due to covalent bonding. This is compensated by the loss of charge from the vacuum regions between lines of atoms (white regions in Figures 6a and 6b with CCD values equal to or less than −0.04). Likewise, the ELF contours in the c-BN slab are highest around the B and N atoms, suggesting electron localization due to covalent bonding.

Figure 6b shows that each N surface ion (white circle) has a contour lobe (dark gray lobe within the interface plane) that is directed toward

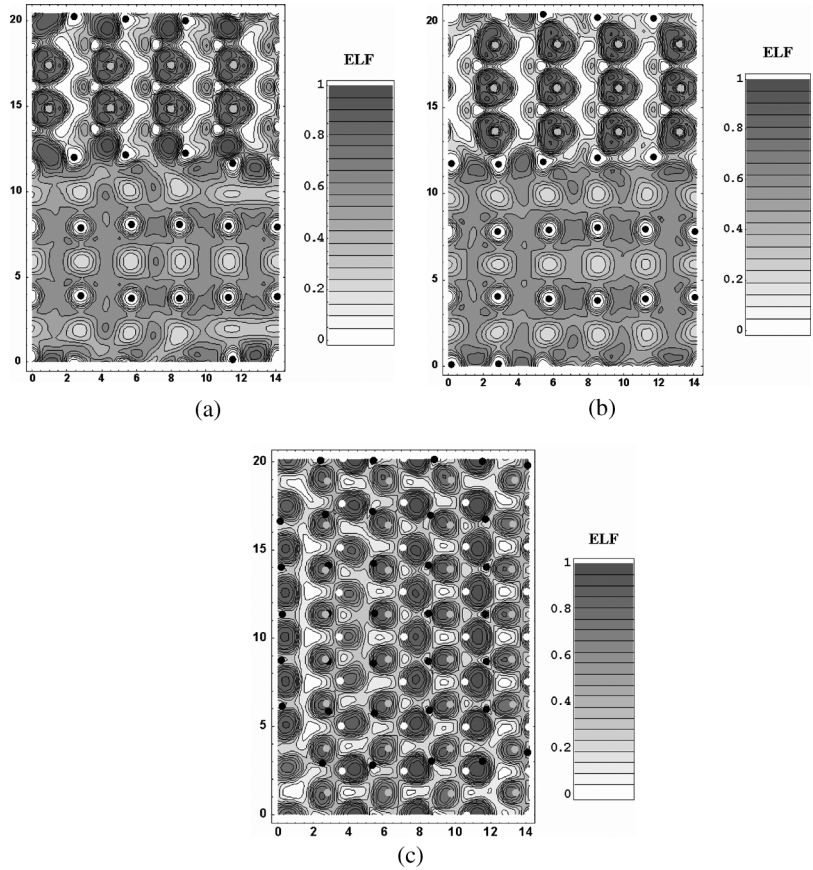

FIGURE 7 ELF plots in the Al(001)–c-BN(110). Dimensions along the sides of the plane denote distance (Å). Al atoms are black; B atoms are white; N atoms are gray. Planes A, B, and C are diagrammed in Figure 2d. a) plane A: Al surface atoms are closest to B surface atoms; b) plane B: Al surface atoms are closest to N surface atoms; c) plane C: plane residing in interface vacuum directly between Al and c-BN slabs.

the interface plane. Charge localization between surface N and Al ions is clearly shown in that lobes are positioned between N and Al surface ions and suggest bonding between Al and N surface ions. Dark gray charge contour lobes within the Al surface plane are indicative of charge compensation due to charge depletion in the Al surface. The ELF value of these lobes in Figure 7b is approximately 0.8 and is slightly less than that observed between Al and B ions in Figure 7a.

The ELF contours between surface B ions and surface Al ions in Figure 7a are ~1. The ELF contour lobes between B and N ions in c-BN represent regions of slightly smaller ELF and weaker covalent bonds. This difference in the ELF contours between Al-B and Al-N pairs suggests that interfacial Al-B bonds have slightly greater covalent character (higher ELF value between the atoms) than Al-N or c-BN bonds. This makes sense as B has three valence electrons, whereas N has five valence electrons. Likewise, the Al-N bonds have slightly greater ionic character than the Al-B or B-N bonds. This difference is also suggested by the corresponding CDD contours. For plane A, the highest CDD values at the interface are directly between Al and B atoms, whereas in plane B, they occur around the N surface ions opposite Al surface ions.

The CDD and ELF contours in plane C (shown in Figures 6c and 7c) are not uniform because of the imperfect interfacial registry between Al and c-BN. For example, there is a preponderance of charge gain lobes in rows between proximate Al–B (*i.e.*, dark gray lobes between white and black circles) and Al–N pairs distributed within the rectangular section 5 Å to 12 Å along the horizontal axes in Figures 6c and 7c. Additional charge is noted in lobes with lighter shading that fall between adjacent rows of Al ions in the Al slab, and these denote regions where charge accumulation is far less than that in the dark gray lobes. We surmise that interfacial bonding likely consists of mixed metallic–covalent–ionic bonds at the interface.

Although the CDD and ELF plots provide a useful qualitative view of bonding within the minimized Al(001)–c-BN(110), quantitative estimates of total charge density and charge redistribution are provided by plots of planar-averaged charge density and planar-averaged CDD. Figure 8 shows the planar-averaged charge density with distance relative to the middle plane in the Al(001) slab. The plot is divided into regions corresponding to the Al and c-BN slabs. Solid circles represent "nominal" planes containing ion cores in each slab. The open circles within the c-BN(110) are interstitial planes. Because of the corrugation in each plane, we averaged the charge density within 1 Å widths such that all atoms within this width resided on the associated plane in the as-built cell. Differences between the charge density and CDD values for the individual slices in our 1 Å widths are in the fourth decimal place (and hence miniscule).

Within the Al slab, the total charge density is approximately 0.16 (same units as CDD) with a slight decrease in the surface layers. Alternatively, the c-BN planes in c-BN(110) have a higher charge density, and the charge diminishes in the interstitial regions (open circles). The charge density is higher in the c-BN slab overall than

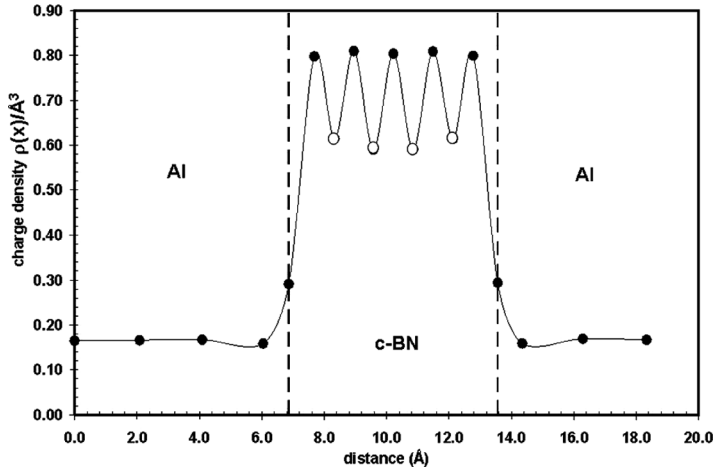

FIGURE 8 Planar averaged charge density plot for Al(001)–c-BN(110).

in the Al slab because of the higher density in the c-BN slab. Dotted lines represent the interface planes, and it is interesting to note that the charge in these planes lies intermediate to that in the Al(001) and c-BN(110) surface planes. Figure 9, which shows the planar-averaged CDD, suggests that the Al surface layers are slightly charge depleted, whereas the c-BN(110) surface layers accumulate charge. We attribute

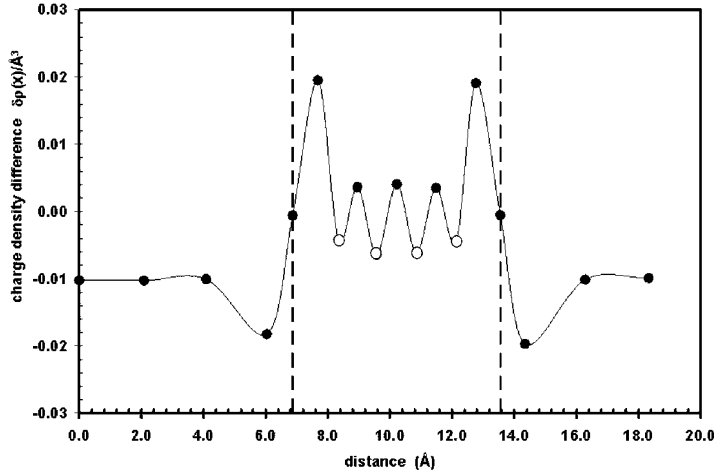

FIGURE 9 Planar averaged charge density difference plot for Al(001)–c-BN(110).

this to the fact that both B and N are more electronegative than Al. Note the relatively small charge accumulation within the interface planes. The internal layers of c-BN accumulate less than one-half the charge accumulated in the surface planes. The results for Al(110)–c-BN(110) were very similar to those for Al(001)–c-BN(110) and are not shown.

8. CLOSING REMARKS

Using a plane wave density functional methodology with the LDA for the exchange and correlation, adhesion was investigated at model Al(001)–c-BN(110) and Al(110)–c-BN(110). Both cells were constructed to be fully periodic, containing single slabs of Al and c-BN. Each cell had the appropriate inversion symmetry to guarantee identical geometric and chemical environments for the two interfaces. Because of the large lattice mismatch among Al(001), Al(110), and c-BN(110), interfacial registry was imperfect, and this led to nonuniform charge distribution and ionic movement within the interfacial planes. The work of separation, W_s, which is indicative of interfacial adhesion, was computed for each cell. For the fully minimized Al(001)–c-BN(110), $W_s = 2.65\,J/m^2$. For the fully minimized Al(110)–c-BN(110), $W_s = 2.25\,J/m^2$. The slightly larger W_s for Al(001)–c-BN(110) is most likely due to the greater number of interplanar Al, B, and N ions. When compared with results from previous adhesion calculations on other interface couples involving Al, the present W_s values suggest that adhesion between Al and c-BN is intermediate to that predicted for Al and VC and for Al and WC (some caution in comparing these results should be exercised because the previous simulations used the GGA for the exchange and correlation functional). Note that VC and WC are similarly hard refractory materials and, like c-BN, are largely covalently bonded. Previous results for Al adhesion to diamond 1×1 suggested transfer of two Al layers to the diamond surface during tensile debonding. Although such simulations were not performed in the present work, we anticipate some Al transfer to c-BN(110) would occur, although significant interfacial charge non-uniformities may not promote transfer of a contiguous Al layer. Corrugation in each layer of the minimized cells was investigated and found (as expected) to be greatest within the Al slab. Bond character was investigated in specific planes within the minimized Al(001)–c-BN(110) cell by displaying contours of the CDD and ELF. Interfacial Al-N and Al-B bonds were inferred from the plots, with some subsurface back-bonding noted in the Al slab due to charge depletion in the surface layers. Because the Al(111) has a similar surface energy to the Al(110) or (001), we surmise

that W_s for Al(111)–c-BN(110) is probably quite close to the values predicted herein.

ACKNOWLEDGMENTS

The National Center for Supercomputing Applications at the University of Illinois at Urbana Champaign provided computational resources through grant number DMR000015N. Additional computational resources were provided by the Fulton High Performance Computing Center at Arizona State University. The Computational Materials Science group at Arizona State University kindly assisted with various aspects of the work. Finally, the VASP authors are gratefully acknowledged for their assistance.

REFERENCES

[1] Wentorf, R. H. Jr., *J. Chem. Phys*. **26**, 956 (1957).
[2] Moeller, T., *Inorganic Chemistry: A Modern Introduction* (John Wiley & Sons, New York, 1982).
[3] Kester, D. J. and Messier, R., *J. Appl. Phys.* **72**, 504–513 (1992).
[4] Lu, M., Bousetta, A., Bensaoula, A., Waters, K., and Schultz, J. A., *Appl. Phys. Lett.* **68**, 622–624 (1995).
[5] Fitz, C., Kolitsch, A., Moller, W., and Fukarek, W., *Appl. Phys. Lett*. **80**, 55–57 (2001).
[6] Reinke, S., Kuhr, M., and Kulisch, W., *Diamond Relat. Mater.* **5**, 508–513 (1996).
[7] Klett, A., Malavé, A., Freudenstein, R., Plass, M. F., and Kulisch, W., *Appl. Phys. A* **69**, 653–656 (1999).
[8] Wang, Y. S., Ping, W., and Ping, L. K., HPC report, CSE Symposium 2003, www.ihpc.a-star.edu.sg/newsletter/vol05issue02.pdf (Accessed December 2005)
[9] Mailhiot, C., Grant, J. B., and McMahan, A. K., *Phys. Rev. B* **42**, 9033–9039 (1990).
[10] Xu, Y. N. and Ching, W. Y., *Phys. Rev. B* **44**, 7787–7798 (1991).
[11] Zunger, A. and Freeman, A. J., *Phys. Rev. B* **17**, 2030–2042 (1978).
[12] Furthmuller, J., Hafner, J., and Kresse, G., *Phys. Rev. B* **50**, 15606–15622 (1994).
[13] Pickett, W. E., *Phys. Rev. B* **38**, 1316–1322 (1988).
[14] Lambrecht, W. R. L. and Segall, B., *Phys. Rev. B* **40**, 9909–9919 (1989).
[15] Lambrecht, W. R. L. and Segall, B., *Phys. Rev. B* **41**, 5409 (1990).
[16] Yamamoto, K., Kobayashi, K., Ando, T., Nishitani-Gamo, M., Souda, R., and Sakaguchi, I., *Diamond Relat. Mater.* **7**, 1021–1024 (1998).
[17] He, G. M., Zheng, Y. M., Wang, R. S., and Li, S. P., *Solid State Commun.* **118**, 287–290 (2001).
[18] Benzair, A. and Aourag, H., *Superlattices Microstruct.* **31**, 219–228 (2002).
[19] Wang, H., Zheng, J., Wee, A. T. S., and Chuan, C. H. A., *J. Elect. Spectr. Rel. Phen.* **114–116**, 483–488 (2001).
[20] Zhang, R. Q., Lo, S. F., Wan, J., Yu, D. K., and Le, S. T., *Comp. Mat. Sci.* **23**, 38–42 (2002).
[21] Watanabe, S., Wheeler, D. R., Abel, P. B., Street, K. W., Miyoshi, K., Murakawa, M., and Miyake, S. *NASA Tech. Briefs* LEW 16695, 1998.
[22] Edgar, J. H., *Properties of Group III Nitrides* (INSPEC, London, 1994).

[23] Tzeng, Y., Yoshikawa, M., Murakawa, M., and Feldman, A., *Proceedings of the 1st International Conference on the Applications of Diamond Films and Related Materials* (Elsevier Science, Auburn, AL, 1991), pp. 143–148.
[24] Kresse, G. and Furthmuller, J., *Phys. Rev. B* **54**, 11169–11186 (1996).
[25] Kresse, G. and Furthmuller, J., *Comput. Mater. Sci.* **6**, 15–50 (1996)
[26] Blochl, P. E., *Phys. Rev. B* **50**, 17953–17979 (1994).
[27] Kresse, G. and Joubert, D., *Phys. Rev. B* **59**, 1758–1775 (1999).
[28] Ceperley, D. M. and Alder, B. J., *Phys. Rev. Lett.* **45**, 566–569 (1980).
[29] Qi, Y., Hector, L. G. Jr., Ooi, N. and Adams, J. B., *Surf. Sci.* **581**, 155–168 (2005).
[30] Siegel, D. J., First Principles Study of Metal-Ceramic Interface, Ph.D. Thesis, University of Illinois at Urbana–Champaign (2001).
[31] Pulay, P., *Chem. Phys. Lett.* **73**, 393 (1980).
[32] Broyden, C. G., *Math. Comp.* **19**, 577–593 (1965).
[33] Johnson, D. D., *Phys. Rev. B* **38**, 12807–12813 (1988).
[34] Hellman, H., *Einfuhrung in die Quantumchemie* (Deuticke, Leipzig, 1937).
[35] Feynman, R. P., *Phys. Rev.* **56**, 340–343 (1939).
[36] Blochl, P. E., Jepsen, O., and Andersen, O. K., *Phys. Rev. B* **49**, 16223–16233 (1994).
[37] Harper, C., *Handbook of Ceramics, Glasses, and Diamonds* (McGraw-Hill, New York, 2001).
[38] Ooi, N. and Adams, J. B., *Surf. Sci.* **574**, 269–286 (2005).
[39] Birch, F., *Phys. Rev.* **71**, 809–824 (1947).
[40] Birch, F., *J. Geophys. Res.* **57**, 227 (1952).
[41] Winter, M. www.webelements.com (Accessed December 2005)
[42] Kittel, C., *Introduction to Solid Physics*, 7th ed. (John Wiley & Sons, New York, 2000).
[43] Ercolessi, F. and Adams, J. B., *Europhys.* **26**, 583–588 (1994).
[44] Simmons, G. and Wang, H., *A Handbook of Single Crystal Elastic Constants and Calculated Aggregate Properties*, 2nd ed. (MIT Press, Cambridge, MA, 1971).
[45] Siegel, D. J., Ph.D. Thesis, University of Illinois at Urbana—Champaign (2001).
[46] Perdew, J. P., Tran, H. Q., and Smith E. D., *Phys. Rev. B* **46**, 11627–11636 (1990).
[47] Skriver, H. L. and Rosengaard, N. M., *Phys. Rev. B* **46**, 7157–7168 (1992).
[48] Vitos, L., Ruban, A. V., Skriver, H. L., and Kollar, J., *Surf. Sci.* **411**, 186–202 (1998).
[49] Kiejna, A., Peisert, J., and Scharoch, P., *Surf. Sci.* **432**, 54–60 (1999).
[50] Venables, J., *Introduction to Surface and Thin Film Processes* (Cambridge University Press, Cambridge, UK, 2000).
[51] Sanchez, B., Jr., *Proceedings of the International Interconnect Technology Conference* **247** (IEEE, 1998).
[52] Heinrichsmeier, H., Fleszar, A., and Eguiluz, A. G., *Surf. Sci.* **285**, 129–141 (1993).
[53] Eustathopoulos, N., Nicholas M. G., and Drevet B., *Wettability at High Temperatures* (Pergamon Press, New York, 1999).
[54] Qi, Y. and Hector, L. G., Jr., *Phys. Rev. B* **69**, 235401–235410 (2004).
[55] Qi, Y., Hector, L. G., Jr., Ooi, N., and Adams, J. B., *Surf Sci.* **581**, 155–168 (2005).
[56] Siegel, D. J., Hector, L. G., Jr., and Adams, J. B., *Acta Mat.* **50**, 619–631 (2002).
[57] Siegel, D. J., Hector, L. G., Jr., and Adams, J. B., *Surf. Sci.* **498**, 321–336 (2002).
[58] Becke, A. D. and Edgecombe, K. E., *J. Chem. Phys.* **92**, 5397–5403 (1990).